SCIENCE CHINA
Technological Sciences

• Article •

January 2016 Vol.59 No.1: 93–108
doi: 10.1007/s11431-015-5947-4

Development and application of a throughflow method for high-loaded axial flow compressors

LI Bo[1,3*], GU ChunWei[1,3], LI XiaoTang[2], LIU TaiQiu[2] & XIAO YaoBing[1]

[1] *Key Laboratory for Thermal Science and Power Engineering of Ministry of Education, Department of Thermal Engineering, Tsinghua University, Beijing 100084, China;*
[2] *Shenyang Engine Design and Research Institute, Shenyang 110015, China;*
[3] *Collaborative Innovation Center of Advanced Aero-Engine, Beijing 100191, China*

Received June 11, 2015; accepted September 6, 2015; published online October 20, 2015

In this paper, a novel engineering platform for throughflow analysis based on streamline curvature approach is developed for the research of a 5-stage compressor. The method includes several types of improved loss and deviation angle models, which are combined with the authors' adjustments for the purpose of reflecting the influences of three-dimensional internal flow in high-loaded multistage compressors with higher accuracy. In order to validate the reliability and robustness of the method, a series of test cases, including a subsonic compressor P&W 3S1, a transonic rotor NASA Rotor 1B and especially an advanced high pressure core compressor GE E^3 HPC, are conducted. Then the computation procedure is applied to the research of a 5-stage compressor which is designed for developing an industrial gas turbine. The overall performance and aerodynamic configuration predicted by the procedure, both at design- and part-speed conditions, are analyzed and compared with experimental results, which show a good agreement. Further discussion regarding the universality of the method compared with CFD is made afterwards. The throughflow method is verified as a reliable and convenient tool for aerodynamic design and performance prediction of modern high-loaded compressors. This method is also qualified for use in the further optimization of the 5-stage compressor.

throughflow method, multi-stage compressor, high-loaded, loss and deviation angle models, streamline curvature, aerodynamic design, performance prediction

Citation: Li B, Gu C W, Li X T, et al. Development and application of a throughflow method for high-loaded axial flow compressors. Sci China Tech Sci, 2016, 59: 93–108, doi: 10.1007/s11431-015-5947-4

1 Introduction

Multistage axial flow compressors are the core components in modern aeroengines and civilian gas turbines. Their performances directly affect the efficiencies of power equipment. Currently, the compressors are undergoing continuous development to achieve higher stage loading with lower aspect ratio blades and higher inlet Mach numbers while maintaining the improvement in efficiency. Swept-curved blade, as an advanced blade modeling method, is also widely applied in latest products [1,2]. The above all make much contribution to flow complexity within blade passages. As a result, it is critical to capture and understand the precise aerodynamic performance during the design and optimization processes of compressors.

Generally speaking, the approach to design and analyze compressor systems can be divided into theoretical and experimental studies [3]. The theoretical framework consists of three parts: One-dimensional method, throughflow method and computational fluid dynamics (CFD).

*Corresponding author (email: libo12@mails.tsinghua.edu.cn)

One-dimensional method focuses on stage and overall characteristics, making it an indispensable tool to check stage matching; nevertheless, it cannot predict the flow details. For the majority of turbomachinery engineers throughflow method and CFD are mostly utilized in daily work.

With the rapid development of computer science and numerical methods, CFD has been widely used to predict the performance and the detailed flow field of compressors [4–6]. However, we should still be aware of its limitations. The unavoidable errors caused by transition and turbulence modeling, blade row interaction, mesh scale and so on will not be overcome in the short term, or "maybe forever" [7–9]; in addition, the shortcomings of CFD are particularly evident in predicting the performance of multistage compressors, causing stage matching and accurate predicting of flow in rear stages to remain major issues for design and optimization [10]. Compared with CFD, the throughflow method is more flexible, systemized and succinct. Much less computing resources and time can be consumed during a throughflow computation [11]. As a major component of the traditional quasi-3D design system, it remains the main tool for aerodynamic design and performance prediction of multistage compressors up to date. Meanwhile, the basic principle of the throughflow method determines that the calculation precision relies heavily on empirical data and correlation models offered by experiments. It is essential to provide reliable data support for calibration and further refinement of the throughflow method by experimental studies; although conducting compressor experiments, especially a full-scale rig test, is complex and costly, and only some key parameters can be got under existing technological conditions.

The throughflow method began with the theory of S1 and S2 stream surfaces proposed by Wu [12] in the 1950s. Many subsequent works were reported in the early years for improving basic theories and establishing functional throughflow computation procedures, e.g., by Smith [13], Swan [14], Novak [15], Bryans and Miller [16], Hirsch and Warzee [17]. Performance prediction models are the core in a practical throughflow computation procedure. The viscous effects are reflected in total pressure loss, deviation angle, blockage, spanwise mixing and so on; thus, the computation accuracy of the procedure depends on various semi-empirical models. For modern high-loaded compressors, the effects of shock and spanwise mixing are both difficult but essential to be simulated. Miller and Hartmann [18] established the first widely used shock loss model with the assumption of a normal shock structure; since then, much optimization and modifications have been performed, such as the work of Oldham [19], Creveling and Carmody [20] and Koch and Smith [21]. In order to avoid the unrealistic entropy increases in the end-wall regions Adkins and Smith [22] and Gallimore and Cumpsty [23] developed two famous individual spanwise mixing models considering the issue in the aspects of secondary flow and turbulent diffusion separately. At present, the throughflow method based on streamline curvature approach plays a critical role in turbomachinery research. Efforts have been made continuously to develop new throughflow methods and more accurate and universal correlation models after fulfillment of substantial experiments and analysis [11,24–34].

In this paper, the authors develop a new engineering platform based on throughflow analysis for the research of a 5-stage compressor which is designed for development of an industrial gas turbine. To meet the requirement of studies regarding the latest turbomachineries, loss and deviation angle models, which have been proven to be credible, are adopted, including a shock model accounting for shock geometry changes with shock loss estimated as a function of inlet relative Mach number, blade section loading, solidity, leading edge radius, and suction surface profile; a spanwise mixing model considering viscous shear force with a no-slip condition; and many other models. The above empirical models and correlations are all tested, and those most suitable are chosen with the authors' experience and adjustments.

To validate the method, a series of test cases is conducted to examine the performances of the method in different aspects. Analyses are first conducted on a subsonic compressor P&W 3S1 and a transonic rotor NASA Rotor 1B to check the basic structure of the computation procedure and the key models, such as the shock model and spanwise mixing model. An advanced high pressure core compressor, GE E^3 HPC, is simulated to provide an overall assessment of the computation procedure afterwards. Then the method is used in the design and analysis of a 5-stage compressor whose full-scale rig test has been performed in Shenyang Engine Design and Research Institute (SEDRI). The numerical results of the overall performance and aerodynamic configuration, both at design- and part-speed conditions, are analyzed and compared with experimental investigations. To further investigate the universality of the method, some discussions about the comparison between throughflow and CFD are performed afterwards.

2 Methodology

The throughflow computation procedure used in the present research is based on the streamline curvature approach. Basically, the method solves the discrete equations of continuity, momentum, energy and state on a computational grid generated in the meridional plane. The geometric features of the compressor also should be taken into consideration. After a series of transformation and simplification the gradients of variables are converted into the direction of the quasi-orthogonal computation station or streamline, as shown in Figure 1.

Next, the governing equations of the streamline curvature

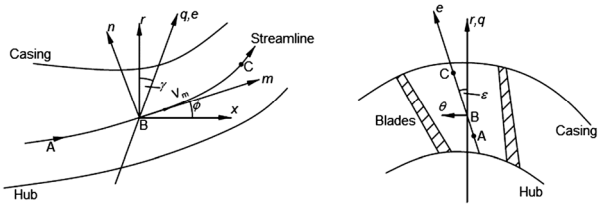

Figure 1 Coordinate system for streamline curvature calculation of meridional flow.

approach can be reorganized as follows.

1) The full radial equilibrium equation:

$$\frac{1}{2}\frac{\partial}{\partial q}V_m^2=\frac{\partial h_0}{\partial q}-T\frac{\partial s}{\partial q}+V_m\frac{\partial V_m}{\partial m}\sin(\phi+\gamma)+\frac{V_m^2}{r_m}\cos(\phi+\gamma)-\frac{1}{2r^2}\frac{\partial}{\partial q}\left(r^2V_\theta^2\right)+\frac{V_m}{r}\frac{\partial}{\partial m}(rV_\theta)\tan\varepsilon. \tag{1}$$

2) The continuity equation:

$$\int_{\text{hub}}^{\text{casing}}\rho V_m\cos(\phi+\gamma)w\mathrm{d}q=\frac{m}{N}, \tag{2}$$

where s is the specific entropy, q is the quasi-orthogonal station, h is the specific enthalpy, $w=2\pi rB/N$, and the meanings of the other symbols have been demonstrated in Figure 1.

The non-linear partial differential eq. (1) is solved by a finite difference approximation, followed by an iterative process. Computation grid nodes are fixed by the intersections of streamlines with quasi-orthogonal computation stations located within and without each blade row. The initial streamline locations are settled such that the annular areas of each stream tube between adjacent streamlines are identical. During one iteration, the calculations are carried out in turn along the quasi-orthogonal computation station, with meridional velocities calculated and iterated to satisfy continuity. Then the new positions for the nodes are adjusted to guarantee that the overall mass flow rate could be divided equally by the streamlines. The next iteration continues afterwards so that the streamlines are relocated time by time until, eventually, their positions remain stable; at this point, the results are output.

The assumptions of inviscid, compressible, adiabatic, steady and axisymmetric flow are made in the radial equilibrium equation, despite the real flow field in the compressors being highly three-dimensional, viscous and turbulent. As mentioned above, empirical models and correlations accounting for viscous effects are indispensable in a throughflow code. In a general throughflow computation procedure the following items are all predicted by different models:

(1) Reference incidence angle;

(2) Deviation angle;

(3) Total pressure loss;

(4) Stall prediction, etc.

The loss prediction, which includes minimum loss calculation and off-design loss calculation, is an important part of the procedure. Generally speaking, the loss sources can be categorized into four groups:

(1) Profile loss;

(2) Endwall loss;

(3) Leakage loss;

(4) Shock loss.

So the minimum loss can be written as

$$\varpi_{\text{ml}}=\varpi_{\text{prof}}+\varpi_{\text{ew}}+\varpi_{\text{leak}}+\varpi_{\text{shock}}. \tag{3}$$

The off-design loss can be calculated with the minimum loss and the difference between the actual incidence and the minimum loss incidence.

$$\varpi=\varpi_{\text{ml}}+c_m\left(i-i^*\right)^2, \tag{4}$$

c_m is the key parameter to the off-design loss prediction and is a function of the blade profile type, Mach number, blade geometric features, and the positive or negative value of $(i–i^*)$.

Different types of models have been tested throughout the authors' work, and final selections are made by their performances in the test cases. Adjustments are also made based on the authors' experiences. For succinctness, this paper will not explain all models in detail; instead, only the ones assumed to be necessary by the authors are presented.

3 Models

3.1 Minimum-loss incidence angle model

The minimum loss incidence angle is of great importance because it is the criterion to define loss and many other parameters. On the basis of lots of cascade flow experiments, Lieblein and Roudebush [35] developed the following widely applied formula:

$$i^*=\left(K_i\right)_{\text{sh}}\cdot\left(K_i\right)_t\cdot\left(i_0\right)_{10}+n\cdot\theta, \tag{5}$$

where $(i_0)_{10}$ is the reference value for the zero-camber, 10% thickness for NACA 65 airfoils. $(K_i)_t$ is the correction factor for a thickness less than 10%. $(K_i)_{\text{sh}}$ is the correction for different blade profiles: $(K_i)_{\text{sh}}$=1 for NACA 65 serious, $(K_i)_{\text{sh}}$=1.1 for C profile and $(K_i)_{\text{sh}}$=0.7 for DCA profile. n is the slope of the change in incidence with the camber angle θ.

As the correlation established by Lieblein is based on the experiments on the low-speed two-dimensional cascade, some revision is necessary for its application in a high-speed compressor. Petrovic et al. [36] added a new calibration factor C_i to the original formula:

$$i^* = (K_i)_{\text{sh}} \cdot (K_i)_{\text{t}} \cdot (i_0)_{10} + n \cdot \theta + C_i, \tag{6}$$

it is found that C_i=2° for NACA serious and C_i=2.5° for DCA profiles can provide the best prediction.

3.2 Deviation angle model

The deviation prediction procedure includes minimum loss deviation calculation and off-design deviation calculation [37]. The minimum loss deviation prediction method used in this paper is the one of Lieblein's [24]:

$$\delta^* = (K_\delta)_{\text{sh}} \cdot (K_\delta)_t \cdot (\delta_0)_{10} + m \cdot \theta, \tag{7}$$

where $(\delta_0)_{10}$ is the reference value for the zero-camber, 10% thickness for NACA 65 airfoils. $(K_\delta)_t$ is the correction factor for thickness less than 10%. $(K_\delta)_{\text{sh}}$ is the correction for different blade profiles: $(K_\delta)_{\text{sh}}$=1 for NACA 65 serious, $(K_\delta)_{\text{sh}}$=1.1 for C profile and $(K_\delta)_{\text{sh}}$=0.7 for DCA profile. m is the slope of the change in deviation angle with the camber angle θ.

Off-design deviation correlation used in this paper is that of Creveling's [38] which relates the $(i–i^*)/\varepsilon_{\text{ref}}$ with $(\delta–\delta^*)/\varepsilon_{\text{ref}}$, among them $\varepsilon_{\text{ref}}=\theta+i^*-\delta^*$.

3.3 Profile loss

Koch and Smith's [21] model, which employs compressible boundary layer theory, is applied to calculate the profile loss. This model connected the loss with an equivalent diffusion factor (D_{eq}^*) accounting for blade thickness, annulus contraction and compressibility effects.

$$D_{eq}^* = \frac{V_{\max}}{V_2} = \frac{V_p}{V_1} \cdot \frac{V_{\max}}{V_p} \cdot \frac{V_1}{V_2}, \tag{8}$$

where V_p is the mean passage velocity in the throat region, $V_{\max}$ is the maximum speed on the suction surface, and the empirical expressions for the first two items on the right side of the equation are given:

$$\frac{V_p}{V_1} = \left\{ \left(\sin\beta_1 - K_1 \sigma \Gamma^* \right)^2 + \left[\frac{\cos\beta_1}{A_p^* (\rho_p / \rho_1)} \right]^2 \right\}^{1/2}, \tag{9}$$

$$\frac{V_{\max}}{V_p} = 1 + K_2 \frac{t_{\max}}{c} + K_3 \Gamma^*. \tag{10}$$

The empirical constants are determined as K_1=0.2445, K_2=0.7688 and K_3=0.6024, and the way to calculate ρ_p/ρ_1, A_p^* and Γ^* can be referred in [21]. Next, the profile loss can be calculated with additional correction for the inlet Mach number, Reynolds number and streamtube convergence values.

3.4 Endwall and leakage loss

Endwall loss is composed of the secondary loss and the annulus loss. Hearsey [39] assumed the annulus loss distribution to be a cubic curve near the endwall.

When $r<r_{\text{mid}}$,

$$\varpi_{\text{hub}} = \varpi_{\text{ml}} \cdot H_{\text{Loss}} \cdot \left[1 - 2 \frac{r - r_{\text{hub}}}{r_{\text{tip}} - r_{\text{hub}}} \right]^3. \tag{11}$$

When $r>r_{\text{mid}}$,

$$\varpi_{\text{casing}} = \varpi_{\text{ml}} \cdot T_{\text{Loss}} \cdot \left[2 \frac{r - r_{\text{hub}}}{r_{\text{tip}} - r_{\text{hub}}} - 1 \right]^3. \tag{12}$$

In the case of the existence of a clearance, the extra influence of the leakage flow should be considered as:

$$\varpi_{\text{tip}} = \varpi_{\text{ml}} \cdot T_{\text{Loss}} \cdot \left[2 \frac{r - r_{\text{hub}}}{r_{\text{tip}} - r_{\text{hub}}} - 1 \right]^3 \cdot \left[1 + \frac{(i - i_{\text{ml}})^2}{(i_{\text{stall}} - i_{\text{ml}})^2} \right]. \tag{13}$$

Hearsey supposed T_{Loss}=0 and H_{Loss}=0 for stators. For the rotors, T_{Loss} equals 1 at the first row and decreases in order by the number of 0.2 in the following rows. H_{Loss} is set according to the experiments.

Howell's [40] model, which has been proven to be accurate by recent researches [41,42] is used to evaluate the secondary loss. The secondary loss is calculated in the form of the drag coefficient; the secondary loss drag coefficient C_{Ds} is given below as a function of the lift coefficient C_L.

$$C_{Ds} = 0.018 C_L^2. \tag{14}$$

The lift coefficient can be calculated as

$$C_L = \frac{2\cos\beta_m}{\sigma} (\tan\beta_1 - \tan\beta_2), \tag{15}$$

where β_m is the average flow angle:

$$\tan\beta_m = \frac{1}{2} (\tan\beta_1 + \tan\beta_2). \tag{16}$$

Then, the total pressure loss coefficient is given as

$$\varpi_{\text{sec}} = \sigma \frac{\cos^2\beta_1}{\cos^3\beta_m} C_{Ds}. \tag{17}$$

Lakshminarayana's [43] model is applied to account for the effects of tip clearance flow. Lakshminarayana divided the loss caused by the leakage into two parts: The loss associated with the induced velocities at the lift line in an inviscid flow and the dissipation of the spanwise flow occurring inside the blade boundary layers near the tip by viscous forces.

The loss coefficients of the two sources (ϖ_u and ϖ_w) are derived as a function of the lift coefficient (C_L), clearance

height (τ), flow angle (β), boundary layer thickness (δ^*), etc.

$$\varpi_u = \left(0.7\frac{C_L^2}{A}\frac{\tau}{s}\right)\cdot\frac{c}{s}\cdot\frac{\cos^2\beta_1}{\cos^3\beta_m}, \tag{18}$$

$$\varpi_w = \frac{\delta_s^* + \delta_p^*}{s}\cdot\frac{1}{A}\cdot\frac{C_L^{3/2}(\tau/s)^{3/2}V_m^3}{V_z V_1^2}. \tag{19}$$

Then the loss is evaluated in the form of a decrease in stage efficiency as shown below, where ψ is the blade loading coefficient and ϕ is the flow coefficient:

$$\Delta\eta = \frac{0.7\cdot(\tau/h)\cdot\psi}{\cos\beta_m}\cdot\left[1+10\sqrt{\frac{\phi}{\psi}\frac{\tau/c}{\cos\beta_m}}\right]. \tag{20}$$

3.5 Shock model

The key point of the shock loss model is to predict the exact structure and location of the shock in the passage. The widely used model was developed by Miller et al. [44], which has been presented in the introduction. However, Bloch et al. [45] found that the structure of the shock varied with different operating conditions, unlike Miller's prediction. Subsequently, Boyer [46] proposed a new model based on the method of Bloch, which also included the method of König et al. [26,27] and Moeckel [47] to determine some key parameters. Boyer assumed three shock structures at different operating conditions (shown in Figure 2), which has been proven to be suitable for transonic stages.

A dual-shock structure (a leading edge detached shock followed immediately by a normal passage shock) is assumed at the peak efficiency operating point. The shape of the detached leading edge shock and the detachment distance can be calculated in Moeckel's way.

With the incidence increasing, the passage shock moves upstream, and the shock angle also undergoes a smooth increase by:

$$SA = SA + \frac{(90^\circ - SA)}{(i_{\text{norm}} - i_{\text{min}})^4}\cdot(i - i_{\text{min}})^4, \tag{21}$$

where SA is the shock angle. The increment of the bow shock loss due to the incidence change also must be considered by

$$\varpi_{\text{bow}} = \varpi_{\text{bow}} + \frac{0.015}{(i_{\text{norm}} - i_{\text{min}})^3}\cdot(i - i_{\text{min}})^3. \tag{22}$$

Eventually, the dual-shock turns to a single detached normal shock at the stall point, and the shock loss can be similarly calculated according to Miller's method at this time.

The angle of the leading edge detached shock remains the same when the incidence decreases and the passage normal shock moves downstream, reaching the outlet of the passage at the choking point. König computed the exit-to-entrance area ratio as

$$\frac{A_{\text{exit}}}{A_{\text{inlet}}} = 0.499\cdot M_{2s} + 0.501 + C_{ar}. \tag{23}$$

The value for C_{ar} is determined to be 0.0774 for MCA or wedge sections, and 0.0351 for precompression sections. Then the Mach number in front of the second normal shock can be calculated, and hence, the total pressure loss can be determined:

$$\varpi_M = \varpi_{M,\text{min}} + \frac{\varpi_{M,\text{choke}} - \varpi_{M,\text{min}}}{(i_{\text{choke}} - i_{\text{min}})^4}\cdot(i - i_{\text{min}})^4. \tag{24}$$

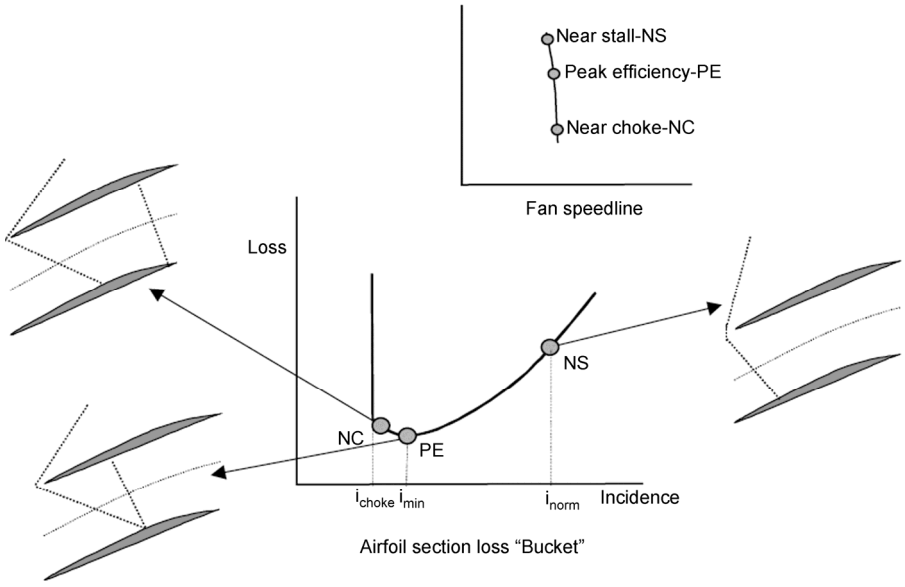

Figure 2 Assumed shock structures at different operating conditions by Boyer [46].

3.6 Spanwise mixing

The spanwise mixing between the endwall flow and main flow is obvious in a multistage compressor, especially for the rear stages. In the present study, a revised version of Gallimore and Cumpsty's [23] model is used in computation stations within and without the blade rows.

Gallimore's model contains the radial heat transfer and shear stresses in the axial and circumferential direction. The changes in entropy, tangential momentum and stagnation enthalpy along streamlines in the mixing process can be calculated, as shown in Figure 3.

The viscous-related terms are as follows.

The dissipation term:

$$\phi = \mu_t \left[\left(\frac{\partial V_z}{\partial r} \right)^2 + \left(\frac{\partial V_\theta}{\partial r} - \frac{V_\theta}{r} \right)^2 \right]. \tag{25}$$

Shear stresses in the circumferential direction:

$$E_\theta = \frac{\partial}{\partial r} \left(\mu_t \left[\frac{\partial V_\theta}{\partial r} - \frac{V_\theta}{r} \right] \right) + \frac{2\mu_t}{r} \left[\frac{\partial V_\theta}{\partial r} - \frac{V_\theta}{r} \right]. \tag{26}$$

Shear stresses in the axial direction:

$$E_z = \frac{1}{r} \frac{\partial}{\partial r} \left[\mu_t r \frac{\partial V_z}{\partial r} \right]. \tag{27}$$

Howard and Gallimore [48] improved Gallimore's model by using a shear force, consistent with a no-slip condition, on the annulus walls in the calculations, which allows for better predictions of the velocity and flow angle profiles near the endwalls.

3.7 Stall prediction

Diffusion factor is a commonly used stall criterion because it represents the boundary layer thickness from which the separated flow near the suction surface trailing edge of a certain blade row can be deduced. However, the diffusion factor has its limitations in predicting compressor instability because studies have shown that the compressor can operate stably with one or more blade rows heavily stalled [10].

Koch [49] established a method to estimate the maximum pressure rise at stall for compressor stages. In his method, a compressor blade passage is simulated as a straight diffuser, and the corrections for Reynolds number, tip clearance, axial spacing and effective dynamic pressure factor are also made. Because Koch's method is more complete in theory, it is used in the current study.

4 Validation

To validate the throughflow computation procedure, three test cases are performed: Pratt & Whitney 3-stage compressor (P&W 3S1), NASA Rotor1B transonic rotor and high pressure compressor for General Electric Energy Efficient Engine (GE E^3 HPC). The cases are chosen for the following reasons.

The three units are typical in different aspects. P&W 3S1 consists of the rear stages of a compressor with obvious spanwise mixing, providing an opportunity to verify the reliability of the basic structure of the computation procedure and the key models, especially the spanwise mixing model. Rotor 1B is a transonic rotor developed for high-loaded compressor, which allows for verification of the applicability of the procedure in transonic stages and validation of the shock model. The method's predictive ability for the overall performance and aerodynamic configuration of a modern high-loaded compressor can be examined on the E^3 HPC, which represents an advanced multistage compressor.

The detailed design and experimental data of the test cases can be obtained in the published literature, enabling careful comparison of the results.

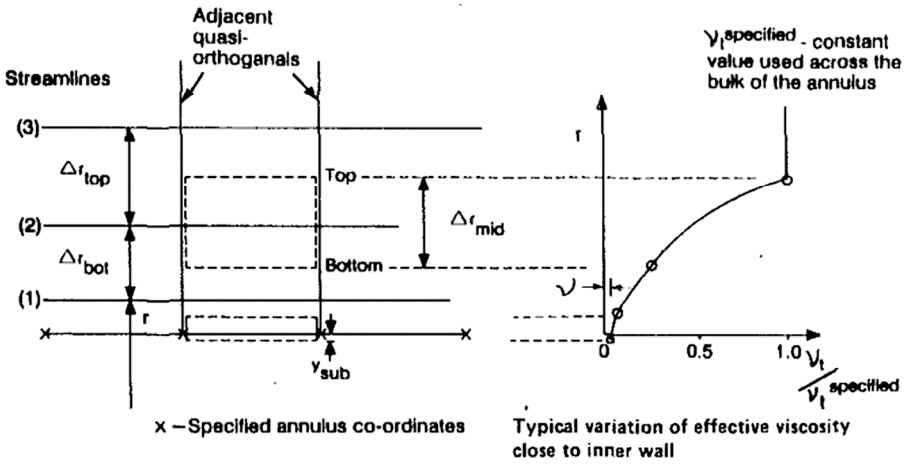

Figure 3 Computational mesh and variation of effective viscosity by Howard [48].

4.1 P&W 3S1

The 3-stage compressor developed by P&W in the 1970s was used to perform research on a high-loaded axial compressor [50,51]. The 3S1 consists of rear stages of a compressor and has relatively low aspect ratio blades, with strong secondary flow and spanwise mixing in the flow field. The design parameters are presented in Table 1.

A total of 21 streamlines in the radial direction and 108 computation stations in the axial direction are used in the throughflow computation, as shown in Figure 4 (for the sake of clarity, only the computation stations are shown in the meridional view of the compressor):

The test data for 85%, 100% and 105% of the design speed are available, including the overall characteristics and the spanwise distributions of outlet fluid properties. Figure 5 shows the performance curves. The results indicate that the procedure can predict the trends of the performance curves accurately. The predicted pressure ratios are only slightly lower than those in the experiments. The relative errors between the computed efficiencies and experimental results are less than 1% for the design point and are acceptable at off-design conditions.

Table 1 Design parameters of P&W 3S1

Items	Value
Pressure ratio	1.357
Rotational speed (rpm)	5455
Corrected airflow (kg/s)	4.30
Isentropic efficiency	0.883
Aspect ratio	0.81
Hub-to-tip ratio	0.915
Average solidity of rotors	1.10

Figures 6 and 7 illustrate the spanwise distributions of the outlet total temperature and the total pressure for different operating conditions at the design speed. With the improved spanwise mixing model, the outlet fluid properties are found to be predicted precisely. All of the above comparisons demonstrate the validity of the basic structure of the computation procedure especially the spanwise mixing model. The shock model will be tested in the following cases.

4.2 NASA Rotor 1B

Rotor 1B is a single rotor test rig developed by NASA in the 1960s to study the performances of transonic rotor blades [52,53]. The detailed measurements of outlet fluid properties enable the validation of the new shock model established by Boyer. The design parameters of Rotor 1B are presented in Table 2.

To better simulate the effects of shock in the flow field, 21 streamlines in the radial direction and 36 computation stations (seven within the blade row) in the axial direction are used as demonstrated in Figure 8.

In the experiments, the fluid properties at 10%, 30%, 50%, 70% and 90% span of the outlet were recorded. To reflect the comprehensive effects of the shock, the radial distributions of the loss coefficient at different operating conditions are compared in Figure 9. The results reveal that whether at the design point or near stall, the distributions of the loss coefficient all agree well with experimental results. The main discrepancies are located at 50% span for a passage vortex induced by the strong shock [53]. Nevertheless, the results of the comparison verify the reliability of the advanced shock model.

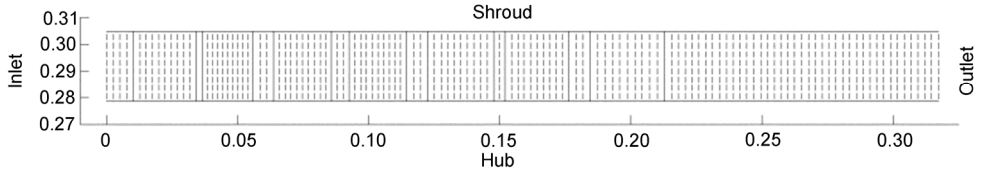

Figure 4 Throughflow computation mesh of P&W 3S1.

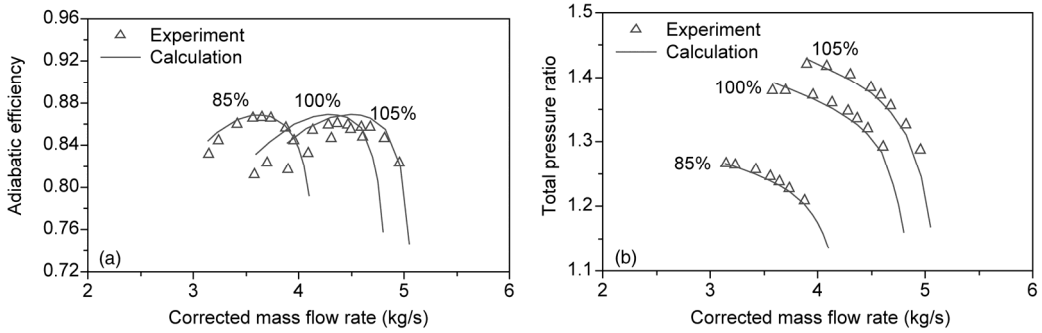

Figure 5 Overall performance of P&W 3S1. (a) Efficiency-mass flow; (b) pressure ratio-mass flow.

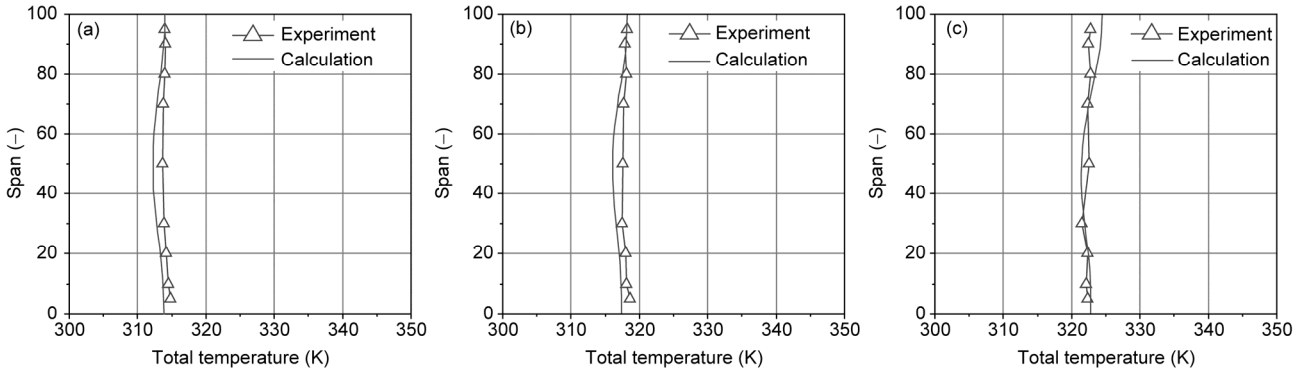

Figure 6 Comparison of outlet total temperature at different operating conditions for P&W 3S1. (a) Near choked; (b) design; (c) near stall.

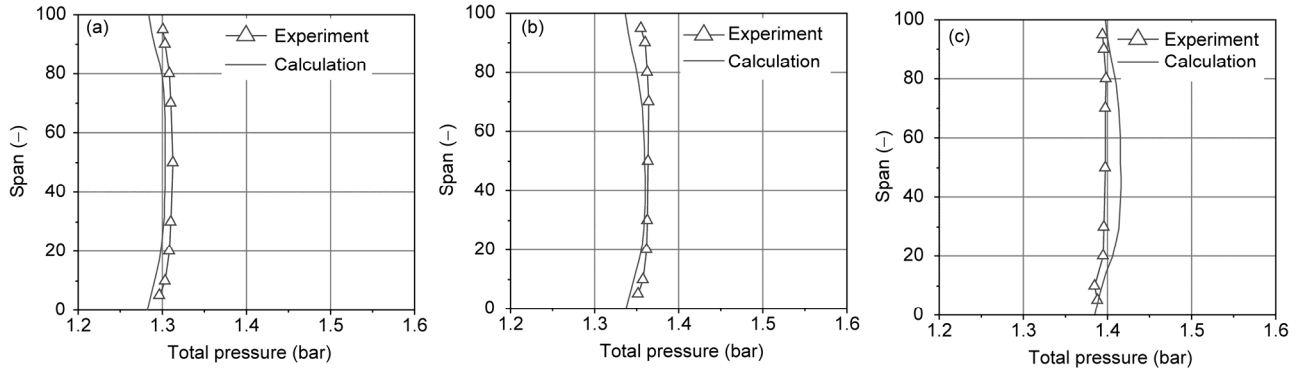

Figure 7 Comparison of outlet total pressure at different operating conditions for P&W 3S1. (a) Near choked; (b) design; (c) near stall.

Table 2 Design parameters of Rotor 1B

Items	Value
Pressure ratio	1.6
Rotational speed (r/min)	8791
Corrected airflow (kg/s)	97.83
Solidity	1.306
Aspect ratio	2.5
Hub-to-tip ratio	0.5
Blade number	44
Tip Mach Number	1.38

4.3 GE E^3 HPC

The research and development of a high pressure compressor for the E^3 aircraft engine by GE in the 1980s was a part of Aircraft Energy Efficiency (ACEE) Program, Energy Efficiency Engine (E^3) Project [54,55]. The 10-stage core compressor was designed to offer the best overall combination of desirable features: compactness, high efficiency, low operation cost and low fuel consumption. The ideal performance of the E^3 HPC has been fully endorsed by industry and it is applied in the new GE90 turbofan engine for Boeing 777. The full-scale rig test results and aerodynamic design parameters provide an opportunity to examine the robustness and reliability of the entire computation procedure in the modern compressor. The geometry and overall design performance of the GE E^3 HPC are presented in Table 3.

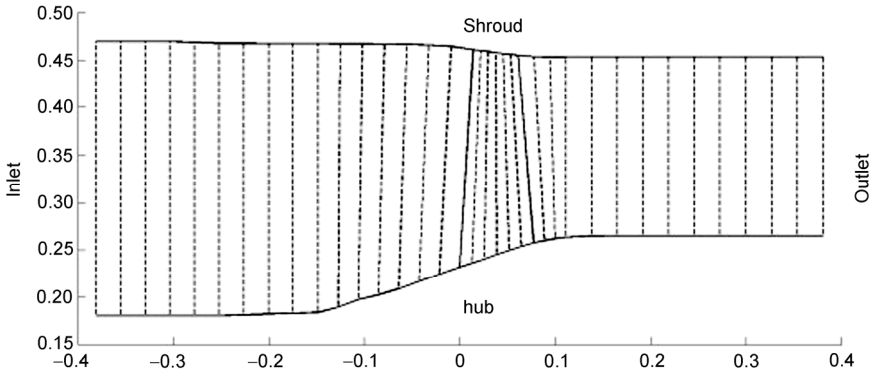

Figure 8 Throughflow computation mesh of Rotor 1B.

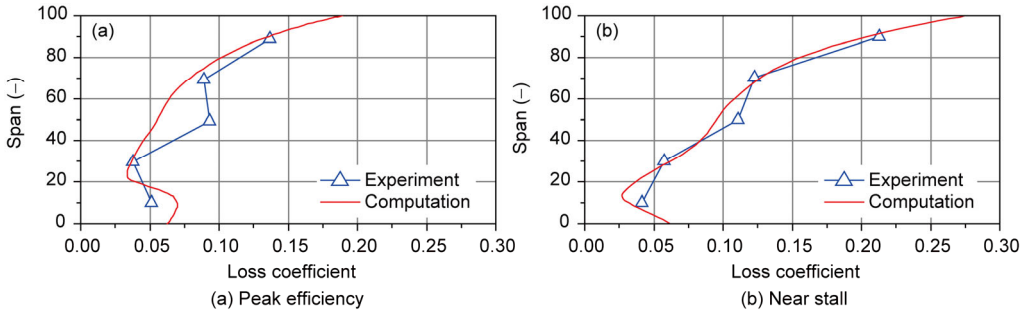

Figure 9 Comparison of loss coefficient at different operating conditions for Rotor 1B.

Table 3 Design parameters of the GE E^3 HPC

Items	Value
Corrected tip speed (m/s)	456
Inlet radius ratio	0.503
Flow/Annulus area (kg/s m^2)	185.5
Corrected airflow (kg/s)	54.4
Tota1 pressure ratio	23
Rotor 10 exit hub speed (m/s)	352.7
OGV exit mach number	0.3
Number of rotors and stators	1672
Average aspect ratio	1.48
Average solidity	1.36
Adiabatic efficiency	0.857
Polytropic efficiency	0.903

Figure 10 shows the computation mesh for the GE E^3 HPC. Twenty-five streamlines in the radial direction and 186 computation stations in the axial direction (including the ones within each blade row) are set.

Figure 11 shows the comparison of the overall performance. At the design point with the total pressure ratio of 23, the discrepancies between the prediction and experiment are found to be quite small. The computational deviations at other operating points are greater, but the overall trend is predicted precisely.

To further check the procedure's ability to predict the aerodynamic configuration, the computed reaction, temperature ratio and pressure ratio of each stage at the design point are compared with the design values, as demonstrated in Figure 12. The results show good agreements.

The validation of the new throughflow method has been conducted in the upper sections, which demonstrates that the computation procedure can provide a quick and accurate prediction for the overall performance and aerodynamic configuration of a modern compressor. The robustness and reliability of the models are also verified.

5 Application on the 5-stage compressor

The throughflow computation procedure is applied to the design and analysis of a 5-stage compressor. The compres-

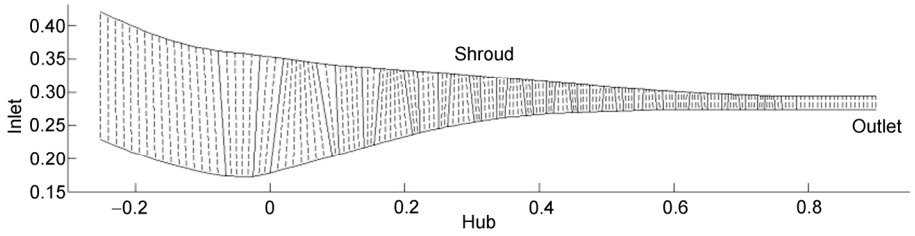

Figure 10 Throughflow computation mesh of GE E^3 HPC.

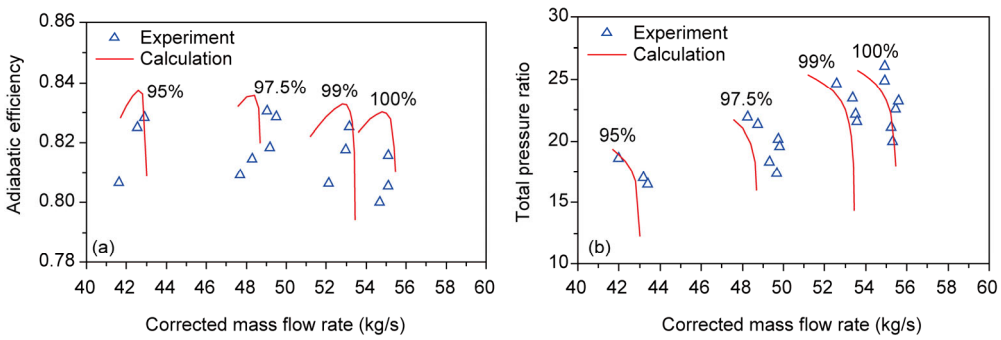

Figure 11 Overall performance of GE E^3 HPC. (a) Efficiency-mass flow; (b) pressure ratio-mass flow.

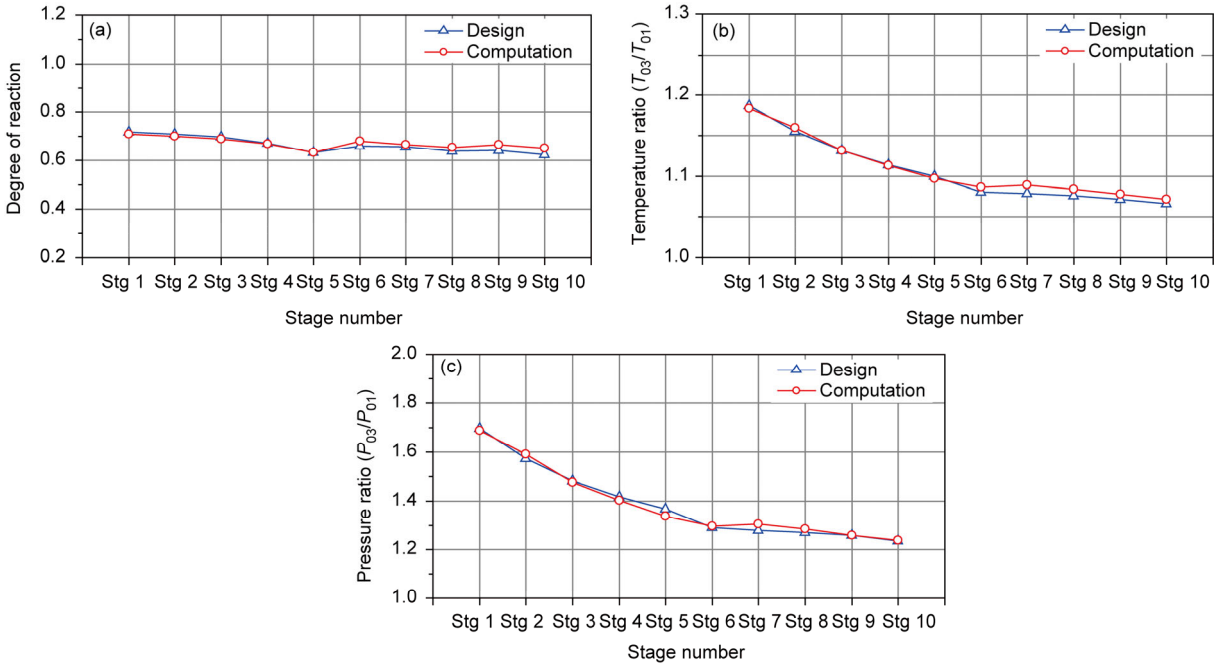

Figure 12 Comparison of stage parameters for GE E^3 HPC. (a) Reaction degree; (b) temperature ratio; (c) pressure ratio.

sor is designed for developing an industrial gas turbine. High-loading design strategy is adopted in its development. MCA airfoils are adopted for the transonic rotors of the first stage, and CDA profile philosophy is adopted in designing the rest subsonic blades. 3D design features, including re-camber and vane bow, are incorporated into the conventional 2D design based on 3D numerical simulations. The first two rows of stators as well as the IGV are variable for surge control at part speed. Recently, the full-scale rig test of the compressor has been performed in SEDRI with several parameters measured under different operating conditions. However, due to the proprietary nature of this information, no detailed design parameters can be provided here.

In order to thoroughly study the aerodynamic configuration of the compressor, 21 streamlines in the radial direction and 108 computation stations in the axial direction are used in the throughflow computation, as shown in Figure 13.

Figure 14 shows the comparison of the overall characteristics between the predictions and experimental results at the design- and off-design speeds, where all data are non-dimensionalized by the design values. The shapes of performance curves predicted by the throughflow method are similar to those of the test ones. At the design speed, the mass flow rate is under-predicted by approximately 1.5%, and the discrepancy between the two peak efficiencies is less than 0.5%. At lower speeds, the discrepancies of the mass flow rate are larger but the trends are still reasonable, considering the installation errors of the adjustable blades during the experiments. According to Koch's stall prediction method, the 5th stage is the first stage turning into stall at each rotating speed, which is also observed in the experiments. To study the detailed flow field when the compressor is approaching stall, more work is required, involving a combination of experiments, CFD and throughflow analysis. However, the computation procedure proves to have a high accuracy in simulating the overall performance of the newly designed compressor. To further validate the code's ability to capture the aerodynamic characteristics of the compressor, the comparisons of aerodynamic configurations are presented below.

The spanwise total pressure distributions at the inlet planes of the rear four stator rows is measured for different operating conditions during the experiments, along with the casing wall static pressure rise between each blade row. The comparisons of the experimental data with the predictions are shown in Figures 15 and 16. The two comparison results

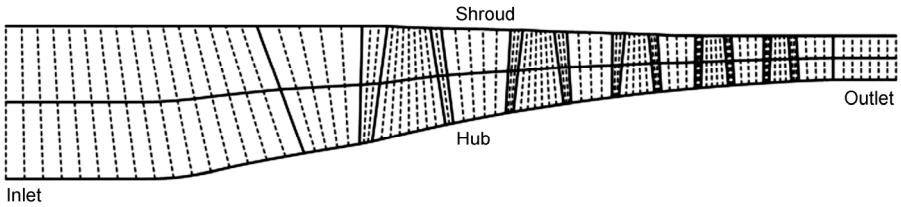

Figure 13 Throughflow computation mesh of the 5-stage compressor.

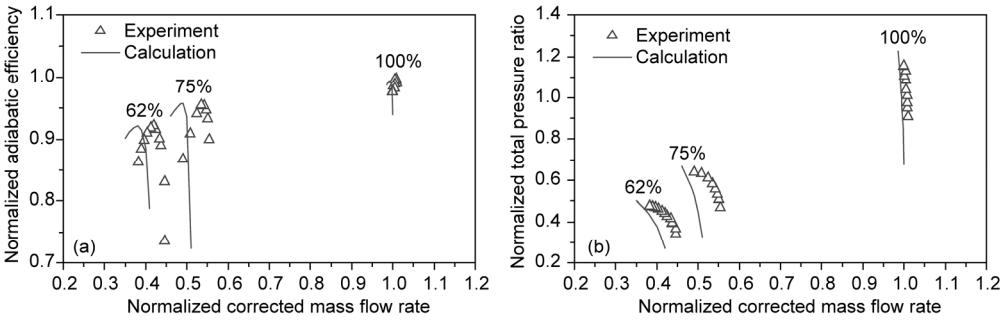

Figure 14 Overall performance of the 5-stage compressor. (a) Efficiency-mass flow; (b) pressure ratio-mass flow.

indicate good agreement between the simulation and the experimental data. The calculated total pressures in front of the four stator rows are in general accord with the experimental data, while the discrepancies occur where the secondary flow is strong. The casing wall static pressure is only under-predicted at the last stage; hence, it can be inferred that the disturbance of the other unit (perhaps influenced by the outlet throttle valve) causes the discrepancy. Conclusively, the newly developed throughflow method is adequate for prediction of the aerodynamic configuration for the modern 5-stage compressor.

6 Further discussion

The above results have validated the effectiveness of the throughflow procedure. To further investigate the universality of the procedure, the throughflow method and CFD are both conducted on a certain single-stage subsonic axial compressor in this work. More discussion is detailed by comparing the computation results with the experiments, attempting to determine the relative advantages and limitations of the method.

The single-stage compressor is equipped with four blade rows: IGV, rotor, stator and OGV. The numerical simulations are conducted under two conditions with different blade settings: The original one and the restaggered one. The restaggered setting is defined as follows: the stagger angles of the stator and the OGV are reduced by 13 degrees and 10 degrees, respectively.

In the throughflow computation, 18 streamlines in the radial direction and 62 computation stations in the axial direction are used while steady three-dimensional flow simulations are performed by solving the compressible Navier-Stokes equations in CFD computation. The CFD solution is based on NUMECA Fine/Turbo. The grid is generated by Autogrid5. The computational mesh consists of 1 765 242 grid nodes with mesh refinement in the rotor and stator domain. The O4H grid topology is used and the multi-grid technique is adopted. The Spalart–Allamaras turbulence model is used to provide the Reynolds stress terms with the y^+ value less than 1 near walls. All of the CFD computations are performed on the High Performance Computer Cluster (HPCC), which allows for parallel computation. The CFD computation of a single case requires approximately 20 CPU hours, which is 100 times as long as that required by a throughflow computation. The computational mesh for the throughflow and CFD are shown respectively in Figures 17 and 18.

Example speedlines for the single-stage compressor are shown in Figure 19, where the pressure rise coefficient versus mass flow coefficient has been plotted. For the original case, the results of the CFD simulation are in better agreement with experimental ones, while the throughflow simulation exhibits a slightly greater slope of the speedline, with the pressure ratio overestimated at the near stall condition. However, the situation is the opposite for the restaggered case, as the throughflow simulation predicts the results well while the CFD fails to capture the trend of the performance curve, especially near stall. Note that the throughflow computation can provide a precise prediction of the surge margin for both cases.

To further investigate the distinct phenomenon, the details of the flow field under the two settings are analyzed and compared. The two operating points, which are regarded to have the same pressure ratio at near stall condition, are chosen (plotted as A in Figure 19(a) and B in Figure 19(b)).

The comparison of points A and B shown in Figure 20 demonstrates that the flow field has significant changes after the blade is restaggered. At the original setting, an obvious low-Mach-number region is observed near the stator hub, which indicates a three-dimensional vortex caused by the boundary layer separation. The low energy fluid passes through the passage and expands, causing a wide range of blockage further downstream to the OGV. After the blades are restaggered, the low energy fluid region near the stator hub is shrunk and the blockage is strongly reduced. In addition, the figure illustrates that there are signs of small separations that do not cause a severe blockage on the suction side of the rotors for both operation points. Considering that the compressor is operating near stall at both points, the phenomenon can be regarded as normal. To examine in detail the complex flow near the stator hub which is the main difference between the two points, the limiting streamlines

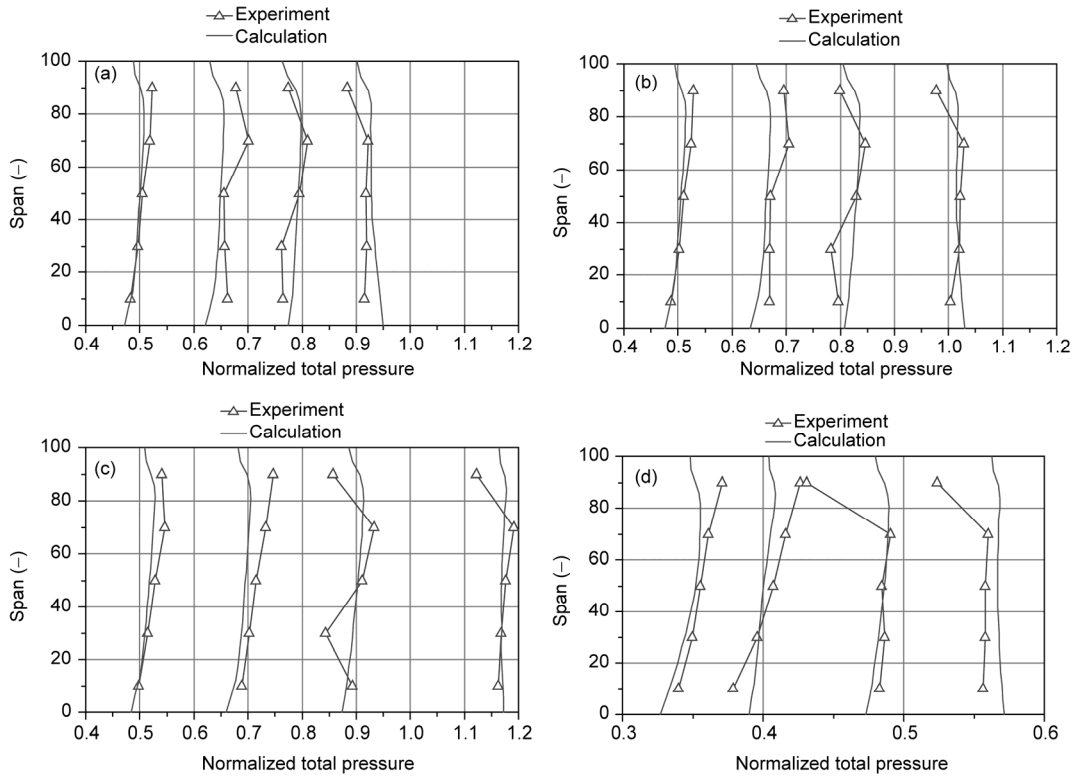

Figure 15 Total pressure profiles at the inlet of rear four stator rows of the 5-stage compressor. (a) Near choked at design speed; (b) design point; (c) near stall at design speed; (d) peak efficiency at 75% design speed.

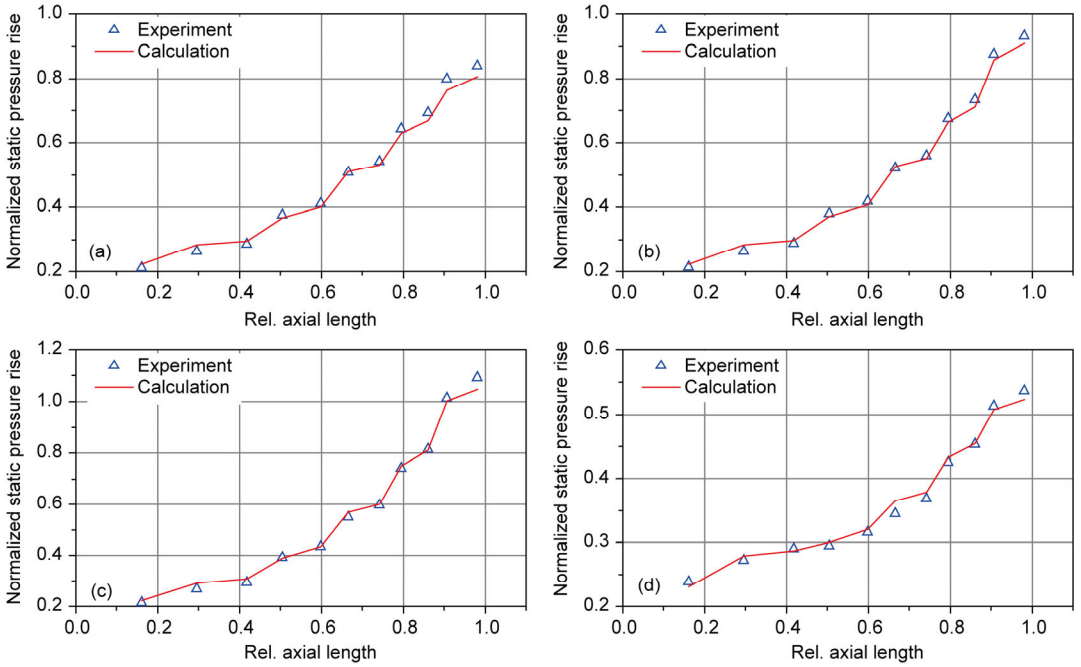

Figure 16 Increase in casing wall static pressure along the 5-stage compressor. (a) Near choked at design speed; (b) design point; (c) near stall at design speed; (d) peak efficiency at 75% design speed.

on the suction surfaces of the rotor and stator are drawn in Figure 21.

The variation of the limiting streamlines on the rotor suction surface between the two operating conditions is relatively small compared with that on the stator surface. The single separation line, which corresponds to the small

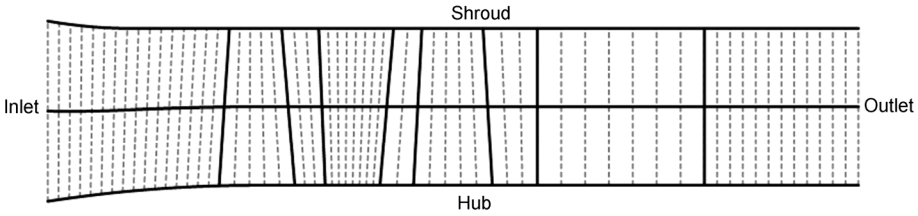

Figure 17 Throughflow computation mesh of the single-stage compressor.

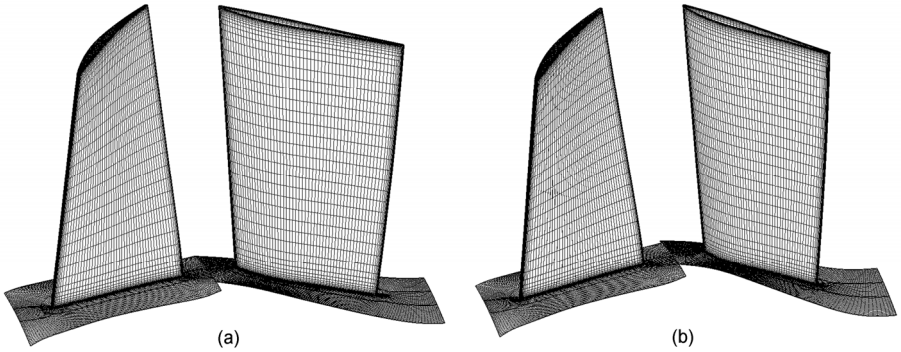

Figure 18 Computational grid for CFD (only the domains of rotor and stator are shown). (a) Original; (b) restaggered.

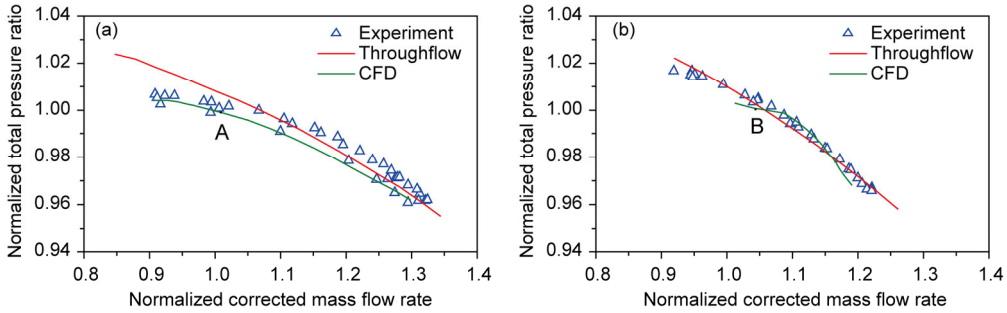

Figure 19 Speedline curves for the single-stage compressor under original and restaggered settings. (a) Original; (b) restaggered.

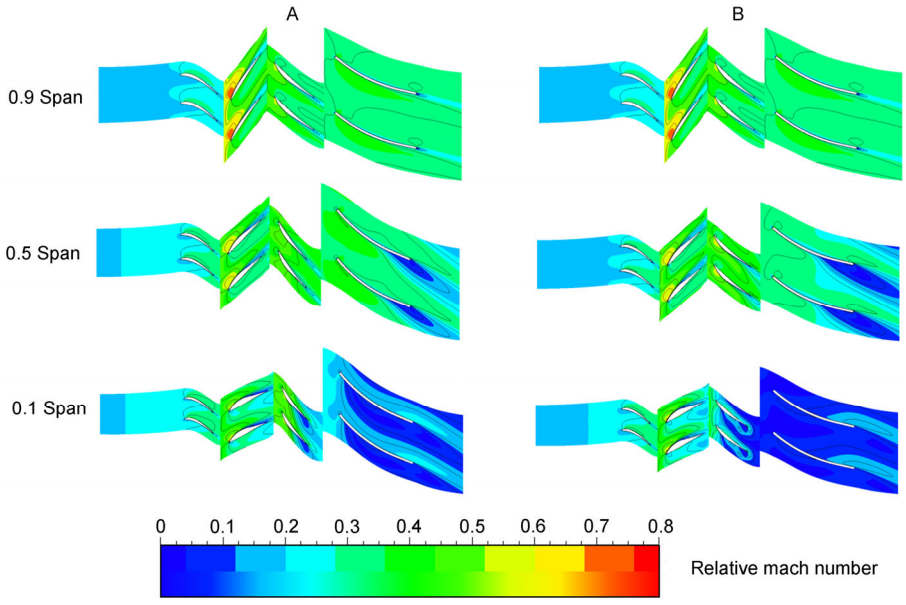

Figure 20 Distribution of relative Mach number for different spans at operating points A and B.

low-speed region shown in Figure 20, starts from the upper side of the blade and extends across nearly the entire span. The starting point at condition A is more upstream, indicating a higher loading on the tip region, which may be the result of a smaller flow rate. The separation on the rotor suction surface under both conditions is confirmed to have a limited effect on the flow state of the rotor passage by combination of Figures 20 and 21. Regarding the stator, the situation is quite different. Under the original setting, bifurcation lines of separation and attachment are found on the lower part of the surface. A focal-type critical point, which indicates a three-dimensional attachment of a vortex, is also observed. The low-energy fluid from the suction boundary layer clearly accumulates and separates into the passage. After interacting with the casing boundary layer, the low-energy fluid converges on the hub-suction corner, thus forming a three-dimensional vortex and causing a large blockage, which corresponds to the computational result shown in Figure 20. This complex flow near the end wall region in the blade passage of a compressor is also defined as a corner vortex. When the blades are restaggered, the separation region moves downwards and greatly decreases. From Figure 21, we can determine that the corner vortex extends from the hub to at most 20% span of the blade at the moment, which is in a good agreement with the distribution of the relative Mach number.

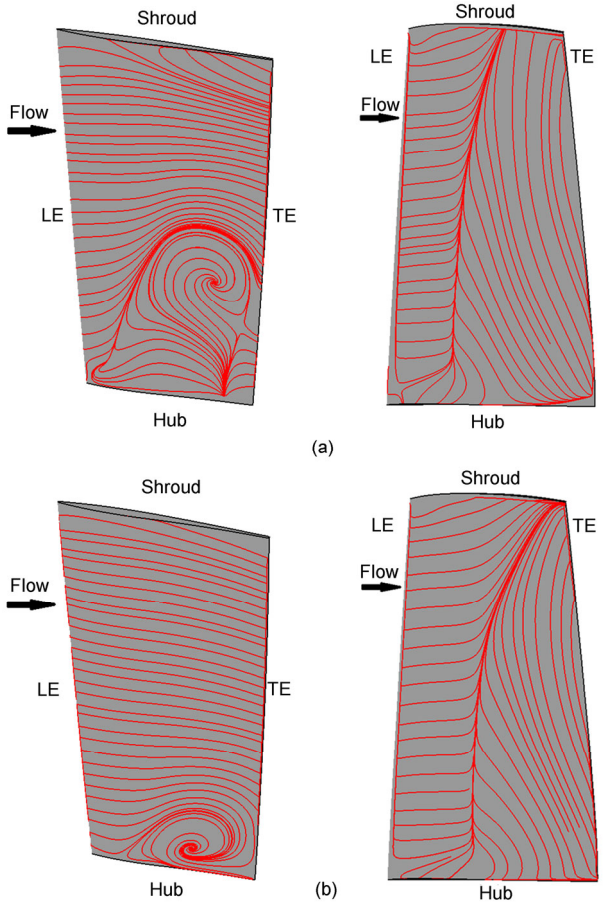

Figure 21 (Color online) Limiting streamlines on blade suction surfaces at two settings. (a) Original; (b) restaggered.

Considering both the flow field and the compressor map together, we gain a deeper understanding regarding the comparative advantage of throughflow compared with CFD. The calculation precision of a throughflow method relies heavily on the correlation models offered by experiments. In addition, most of the algebraic models are based on basic 2D correlations with additional corrections for 3D flow effects, such as the complex secondary flow. In this study, a severe separation occurs on the lower side of the stator suction surface, causing a complicated corner vortex which is beyond the models' predictive ability. This complex flow behavior explains the observation that the throughflow simulation overestimates the pressure ratio at near stall condition for point A when the blockage caused by the corner vortex significantly increases the viscosity loss and weakens the pressure rise. The discrepancies caused by the same reason are also observed in Figure 15: The deviations between the throughflow computation and the experiments are mainly located near the tip region where the secondary flow is strong. However, the throughflow can predict the working characteristics of the compressor better than CFD under other circumstances. Most notably, for the restaggered case, the CFD calculation does not provide converged solutions below the mass flow rate, which is far from the surge line in the experiment. The use of the unsteady calculation may fix the problem, but the time consumed could be an order of magnitude longer. In addition, as a result of its basic principle, the calculation precision of the CFD relies on many factors and is difficult to handle compared with that of the throughflow analysis, which is based on experimental data. Although its ability to capture the effects of complex 3D flow is insufficient in certain cases, the throughflow analysis can offer a fast and precise solution for predicting the overall performance and aerodynamic configuration of the compressors on the whole, making it an indispensable component of the quasi-3D design and analysis system for turbomachinery.

7 Conclusion

A new engineering platform for throughflow analysis based on streamline curvature approach on the S2 streamline surfaces is developed for the research of a 5-stage compressor which is designed for developing an industrial gas turbine. The improved high applicability loss and deviation angle models are integrated into the calculation procedure to accurately reflect the influences of the three-dimensional internal flow. Different models are tested and chosen based on the authors' adjustments to meet the demand of research into advanced high-loaded compressors. Several test cases of modern compressors are conducted to validate the robustness of the method; and the results demonstrate its reli-

ability for turbomachinery design.

The throughflow method is applied in the design and analysis of a 5-stage compressor. The overall characteristics and fluid property profiles along the flow path at both design- and part-speed conditions obtained in the experiments are compared in detail with the computed data. The results validate that the overall performance and aerodynamic configuration can be predicted fast and precisely, and the method is also qualified for further refinement of the 5-stage compressor.

Further discussion is made by the comparison of throughflow analysis with CFD on a certain single-stage subsonic axial-flow compressor, which provides more details on the applicability of the throughflow analysis. Based on the experimental data, the details of the flow field are analyzed. The throughflow method proves to be time-saving and sufficiently precise compared with CFD.

The developed throughflow method is demonstrated to be a powerful tool in aerodynamic analysis for modern compressors; hence, the indispensability of the two-dimensional throughflow method in the compressor studies is further confirmed. Additional studies are necessary to enable the throughflow method to achieve a higher precision for predicting the complex flow near the endwall regions.

This work was supported by SEDRI, and the National Natural Science Foundation of China (Grant No. 51136003). The authors wish to thank SEDRI for permission to publish this paper.

1 Gümmer V, Wenger U, Kau H P. Using sweep and dihedral to control three-dimensional flow in transonic stators of axial compressors. J Turbomach, 2001, 123: 40–48
2 Song Y, Gu C W. Effects of curvature continuity of compressor blade profiles on their performances. ASME Turbo Expo 2014, Düsseldorf, 2014, GT2014-25804
3 Cumpsty N A. Some lessons learned. J Turbomach, 2010, 132: 041018.1–7
4 Gbadebo S A, Cumpsty N A, Hynes T P. Three-dimensional separations in axial compressors. Jurbomach, 2005, 127: 331–339
5 Huang D G, Wu G Q. Preliminary study on the aerodynamic characteristics of an adaptive reconfigurable airfoil. Aerosp Sci Technol, 2013, 27: 44–48
6 Wang Y, Sun X J, Dai Y J, et al. Numerical investigation of drag reduction byheat-enhanced cavitation. Appl Therm Eng, 2015, 75: 193–202
7 Lichtfuss H J. Customized profiles—The beginning of an era: a short history of blade design. ASME Turbo Expo 2004, Vienna, 2004, GT2004-53742
8 Hao Z, Gu C, Song Y. Discontinuous galerkin finite element methods for numerical simulations of thermoelasticity. J Therm Stresses, 2015, 38: 983–1004
9 Denton J, Dawes W. Computational fluid dynamics for turbomachinery design. P I Mech Eng C-J Mec, 1998, 213: 107–124
10 Cumpsty N A. Compressor aerodynamics. London: Longman Scientific & Technical, 1989, 93–131
11 Boyer K M. An improved streamline curvature approach for off-design analysis of transonic compression systems. Dissertation of Doctor Degree. Blacksburg: Virginia Polytechnic Institute and State University, 2001
12 Wu C H. A general theory of three-dimensional flow in subsonic and supersonic turbomachines of axial-, radial, and mixed-flow types. NACA-TN-2604. NACA, 1952
13 Smith L. The radial-equilibrium equation of turbomachinery. J Eng Power, 1966, 88: 1–11
14 Swan W. A practical method of predicting transonic-compressor performance. J Eng Power, 1961, 83: 322–330
15 Novak R. Streamline curvature computing procedures for fluid-flow problems. J Eng Power, 1967, 89: 478–490
16 Bryans A, Miller M. Computer program for design of multistage axial-flow compressors. NASA-CR-54530, NASA, 1967
17 Hirsch C, Warzee G. A finite-element method for through flow calculations in turbomachines. J Fluid Eng, 1976, 98: 403–415
18 Miller G R, Hartmann M J. Experimental shock configurations and shock losses in a transonic-compressor rotor at design speed. NACA RM-E58A14B. NACA, 1958
19 Oldham R K. Some design data for double circular arc compressor blading. NGTE Note NT. 589, 1965
20 Creveling H F, Carmody R H. Axial flow compressor computer program for calculating off-design performance (Program IV). NASA-CR-72427, NASA, August 1968
21 Koch C, Smith L. Loss sources and magnitudes in axial-flow compressors. J Eng Power, 1976, 98: 411–424
22 Adkins G G, Smith L H. Spanwise mixing in axial-flow turbomachines. J Eng Power, 1982, 104: 97–110
23 Gallimore S J, Cumpsty N. Spanwise mixing in multistage axial flow compressors. II: Throughflow calculations including mixing. J Turbomach, 1986; 108: 2–16
24 Lieblein S. Loss and stall analysis of compressor cascades. ASME J Basic Eng, 1959, 81: 387–400
25 Cetin M, Uecer A, Hirsch C, et al. Application of modified loss and deviation correlations to transonic axial compressors. AGARD-R-745, Advisory Group For Aerospace Research and Development Neuilly-Sur-Seine (Fran Ce), 1987
26 Konig W, Hennecke D, Fottner L. Improved blade profile loss and deviation angle models for advanced transonic compressor bladings. 1. A model for subsonic flow. J Turbomach, 1996, 118: 73–80
27 Konig W, Hennecke D, Fottner L. Improved blade profile loss and deviation angle models for advanced transonic compressor bladings. 2. A model for supersonic flow. J Turbomach, 1996, 118: 81–87
28 Pachidis V, Pilidis P, Templalexis I, et al. An iterative method for blade profile loss model adaptation using streamline curvature. J Eng Gas Turb Power, 2008, 130: 011702.1–8
29 Li H B, Gu C, Song Y. Through-flow calculation with a cooling model for cooled turbines. P I Mech Eng A-J Pow, 2015, doi: 0957650915594294
30 Turner M G, Merchant A, Bruna D. A turbomachinery design tool for teaching design concepts for axial-flow fans, compressors, and turbines. ASME Turbo Expo 2006, Barcelona, 2006, GT2006-90105
31 Petrovic M V, Wiedermann A, Banjac M B. Development and validation of a new universal through flow method for axial compressors. P I Mech Eng A-J Pow, 2010, 224: 869–880
32 Song Y, Gu C W, Xiao Y B. Numerical and theoretical investigations concerning the continuous-surface-curvature effect in compressor blades. Energies, 2014, 7: 8150–5177
33 Song Y, Gu C W, Ji X X. Development and validation of a full-range performance analysis model for a three-spool gas turbine with turbine cooling. Energy, 2015, 89: 545–557
34 Wang J, Gu C, Sunden B A. Conjugated heat transfer analysis of a film cooling passage with different rib configurations. Int J Numer Method H, 2015, 25: 841–860
35 Lieblein S, Roudebush W H. Theoretical loss relations for low-speed two-dimensional-cascade flow. NACA TN 3662, NACA, 1956
36 Petrovic M V, Wiedermann A, Banjac M B. Development and validation of a new universal through flow method for axial compressors. ASME Turbo Expo 2009, Orlando, 2009, GT2009-59938
37 Carter A. The low speed performance of related aerofoils in cascade. ARC CP29, His Maj. Stat. Office, 1950

38 Creveling H F, Carmody R H. Axial flow compressor computer program for calculating off-design performance. NASA-CR-72472, NASA, 1968
39 Hearsey R M. Program HT0300 NASA 1994 version. D6-81569TN, 1994
40 Howell A. Fluid dynamics of axial compressors. P I Mech Eng, 1945, 153: 441–452
41 Fouflias D, Gannan A, Ramsden K, et al. Experimental investigation of the influence of fouling on compressor cascade characteristics and implications for gas turbine engine performance. P I Mech Eng A-J Pow, 2010, 224: 1007–1018
42 Eftari M, Jouybari H J, Shahhoseini M R, et al. Performance prediction modeling of axial-flow compressor by flow equations. J Mech Res Appl, 2011, 3: 49–55
43 Lakshminarayana B. Methods of predicting the tip clearance effects in axial flow turbomachinery. J Basic Eng, 1970, 92: 467–482
44 Miller G R, Lewis G W, Hartmann M J. Shock losses in transonic compressor blade rows. J Eng Power, 1961, 83: 235–242
45 Bloch G S, Copenhaver W W, O'Brien W F. A shock loss model for supersonic compressor cascades. J Turbomach, 1999, 121: 28–35
46 Boyer K M O'Brien W F. An improved streamline curvature approach for off-design analysis of transonic axial compression systems. ASME Turbo Expo 2002, Amsterdam, 2002, GT2002-30444
47 Moeckel W E. Approximate method for predicition form and location of detached shock waves ahead of plane or axially symmetric bodies, NACA TN 1921, NACA, 1949
48 Howard M, Gallimore S. Viscous throughflow modeling for multistage compressor design. J Turbomach, 1993, 115: 296–304
49 Koch C. Stalling pressure rise capability of axial flow compressor stages. J Eng Power, 1981, 103: 645–656
50 Burdsall E A, Canal E, Lyons K A. Core compressor exit stage study-1: Aerodynamic and mechanical design. NASA CR-159714, NASA, 1979
51 Behlke R F, Burdsall E A, Canal E, et al. Core compressor exit stage study-2: Final Report. NASA CR-159812, NASA, 1979
52 Seyler D, Smith L. Single stage experimental evaluation of high Mach number compressor rotor blading, part 1: Design of rotor blading. NASA CR-54581, NASA, 1967
53 Seyler D, Gestolow J. Single stage experimental evaluation of high Mach number compressor rotor blading, part 2: Performance of Rotor 1B. NASA CR-54582, NASA, 1967
54 Wisler D, Koch C, Smith L. Preliminary design study of advanced multistage axial flow core compressors. NASA CR-135133, NASA, 1977
55 Holloway P, Koch C, Knight G, et al. Energy efficient engine. High pressure compressor detail design report. NASA CR-165558, NASA, 1982